Earth and Planetary Science Letters, 107 (1991) 523–538
Elsevier Science Publishers B.V., Amsterdam

[DT]

Sediment loading on the Western Platform of the New Zealand continent: Implications for the strength of a continental margin

W.E. Holt * and T.A. Stern

Department of Scientific and Industrial Research, Geology and Geophysics Division, Box 1320, Wellington, New Zealand

Received November 17, 1990; revision accepted September 13, 1991

ABSTRACT

Mechanical properties of the New Zealand lithosphere are determined by forward modelling the gravity and isostatic response of a Plio-Pleistocene sediment loaded shelf margin. The Giant Foreset Formation on the Western Platform of New Zealand is a 2 km thick, 250 km long, and 100 km wide sediment package. Both the downward flexed Pliocene–Miocene boundary beneath the package and a 35–50 mGal peak-to-trough gravity anomaly over the sediment package are best matched with a flexural rigidity in the region of 5.6×10^{22}–1.5×10^{23} N m (effective elastic thickness T_e = 20–28 km). The Giant Foresets are a particularly important load to model because, unlike most sediment-loaded passive margins, there is a time gap of about 70–80 Ma between rifting and subsequent deposition of the sedimentary load. Furthermore, the width of the Giant Foreset load is sufficiently small to afford a reasonable resolution of T_e.

1. Introduction

Our present knowledge of the strength and mechanical properties of the lithosphere depend primarily on analysing the isostatic response to loads created by volcanism, thrust mountain building, ice sheets, or sedimentation at a continental margin. From analyses of the flexure accompanying seamount loading (e.g. [1]) there has emerged a clear understanding of the rigidity of oceanic lithosphere and how rigidity increases with effective thermal age (here thermal age refers to the time since the last major thermal or orogenic event). Rigidity can be parameterised by the effective elastic thickness, T_e, which for oceanic regions generally varies between 5 and 40 km [1].

Establishing an empirical relationship between T_e and thermal age for the continents is proving far more difficult than for the oceans (e.g. [2]). Because of its varied and complicated history, and, in many cases, its much greater age, continental lithosphere shows a wider range of T_e values (5–130 km) [3–11]. Rigidity in continental lithosphere is, however, thought to have a first order dependence on thermal age, [12], and a plot of rigidity versus age for continents is best explained by a 250 km thick cooling plate model, in which T_e is controlled by the depth to the 450 °C isotherm [13].

Karner and Watts [5], Fowler and McKenzie [14] and Watts [15] examined the lithospheric strength of sediment-loaded, Atlantic-type continental margins (e.g., Northwestern Australia, Lord Howe Rise (New Zealand), and the Eastern United States). Gravity modelling of the sediment loads indicate low effective elastic thicknesses along these continental margins. In all locations sedimentation began immediately after continental rifting when the lithosphere was still weak, and significant portions of the total thicknesses accumulated while the lithosphere was thermally young. In contrast, the loading problem analysed here is quite different. The Giant Foreset Forma-

* Now at: Department of Earth and Space Science, State University of New York at Stony Brook, Stony Brook, NY, USA

tion was deposited onto the Western Platform of New Zealand in a short time interval (3–4 m.y.), 60–70 m.y. after the passive margin was formed [16]. Therefore, the analysis of rigidity presented in this paper acts as an important complement to studies of Atlantic-type margins in that the rigidity we obtain from the analysis pertains to continental lithosphere with a thermal age of between 70–80 Ma, rather than to a very young age, or an average age that may span several tens of millions of years after rifting.

In this paper we utilise a diverse body of public-domain data, including paleobathymetry, seismic stratigraphy and marine gravity, to analyse the flexural response of the New Zealand continental lithosphere to the Giant Foresets Formation load. In the last part of the paper we analyse the importance of load width for the resolution of T_e on a sediment-loaded continental margin.

2. Late Cretaceous–Cenozoic history of the New Zealand continental lithosphere

The New Zealand continental lithosphere is predominantly submarine and comprises juxtaposed Paleozoic to Cretaceous terranes [17]. Figure 1 shows the 2000 m isobath, which roughly outlines the extent of New Zealand continental lithosphere. Petroleum drillhole evidence, and onshore geological mapping, show that the Western Platform (Fig. 2), the locality of the Giant Foreset Formation deposition [16], is underlain by the oldest (early Paleozoic) terrane [18]. In the Late Cretaceous the western side of the New Zealand continent separated from Australia, and the Tasman Sea developed by seafloor spreading [19]. Seafloor spreading also occurred on the eastern side of the continent at about 80–60 Ma [20] when New Zealand separated from West Antarctica. Non-marine sediment-filled NNE-trending Late Cretaceous half grabens on the Western Platform [16, 21, 22] are thought to be the result of deformation associated with the opening of the Tasman Sea [23, 24].

Subsidence curves from the Taranaki and Western Platform regions (e.g., Fig. 3) show a classic thermal subsidence of about 2–3 km, or about 1 km when the subsidence associated with sediment loading is back-stripped [25,26]. This

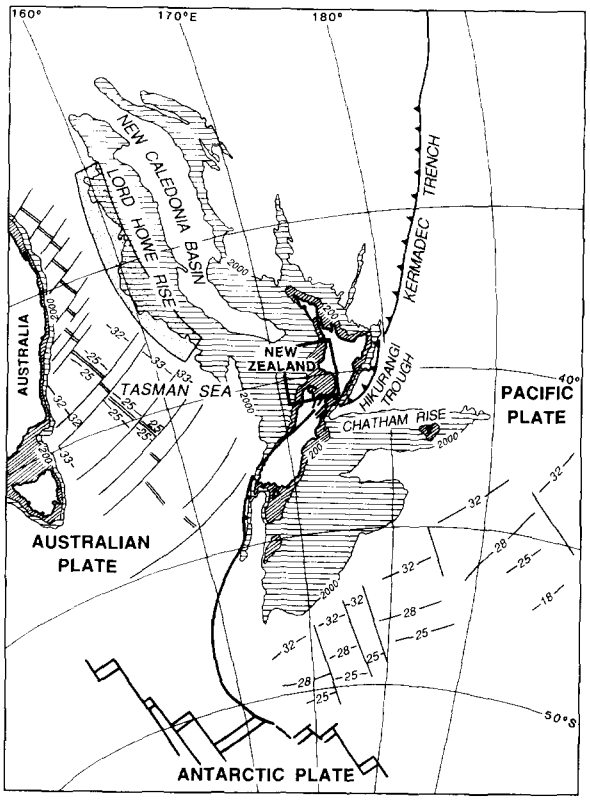

Fig. 1. Location map of study region within New Zealand. 200 and 2000 m contours are indicated. The 2000 m contour shows the approximate extent of the New Zealand continental lithosphere. Magnetic anomalies from the separation of New Zealand from Australia and Antarctica are indicated [53]. Stippled box along Lord Howe Rise Margin shows study region of Karner and Watts [5]. Heavy boxed area outlines study area shown in Fig. 2.

subsidence occurred in the time period 80–30 Ma, and implies, assuming thermal properties equivalent to those used by McKenzie [27], a stretching factor (b) of about 1.5–2. Hence the now 25–30 km thick crust on the Western Platform [26], on the basis of a uniform stretching model [27], would once have been 40–50 km thick.

During the period of thermal subsidence, following the opening of the Tasman Sea, the region of Taranaki and the Western Platform evolved as a passive margin, and was a shallow-marine slope that gradually deepened to the northwest [16,22,28]. Subsidence curves in the Taranaki region show a dramatic shift at around 30–25 Ma (see paleobathymetry in Fig. 3). This rapid subsidence corresponds in time to the beginning of

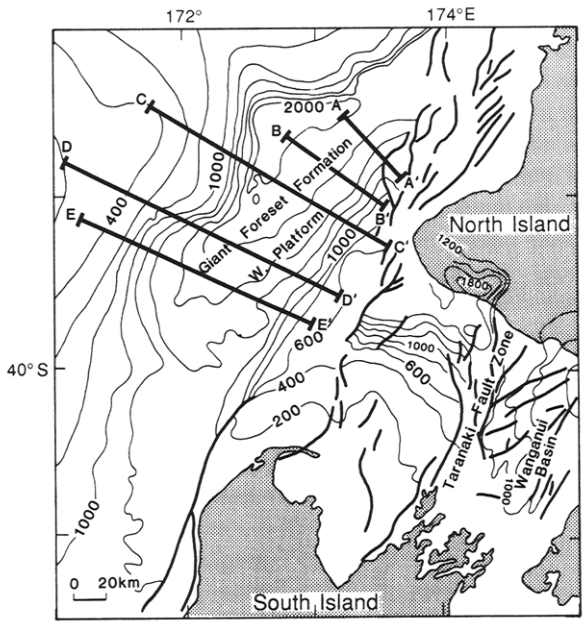

Fig. 2. Isopach map of the Plio-Pleistocene sediment thicknesses, after [31]. The Giant Foreset Formation, just west of North Island, is up to 2000 m thick. Cross sections A–A', B–B' and C–C' were stacked and averaged to provide the structure of the top of the Micoene surface shown in Figs. 5b and 8a. Cross sections D–D' and E–E' were stacked and averaged to provide top of the Miocene structure shown in Figs. 5c and 8b.

subduction beneath the North Island of New Zealand (e.g., [29]) and marks the introduction of a compressional component into the plate boundary zone [30]. A significant component of the observable Miocene shortening occurred in the vicinity of the Taranaki Boundary Fault [16] (Fig. 2). This fault marks the eastern boundary of the South Taranaki Basin [21], which in the Miocene received up to 4 km of sediment [31]. Deep seismic evidence suggests that the South Taranaki Basin developed as a retroarc foreland basin during the Miocene [26]. Therefore, the subsidence observed in all the Taranaki wells at around 30–25 Ma is thought to be related to plate flexure and loading, 150 km east of the Western Platform, rather than a thermal or stretching event [26].

Exploration wells [25] show that areas near the thrust front (Taranaki Fault, Fig. 4) received sedimentation during and after the period of rapid subsidence. Areas 60–100 km west of the thrust front received significant sedimentation only after the subsidence was complete. However, the region of Giant Foreset Formation deposition, 160 km west of the thrust front, was relatively starved of Miocene sediment (Fig. 3). Therefore, at the end of the Miocene the inital contitions for the

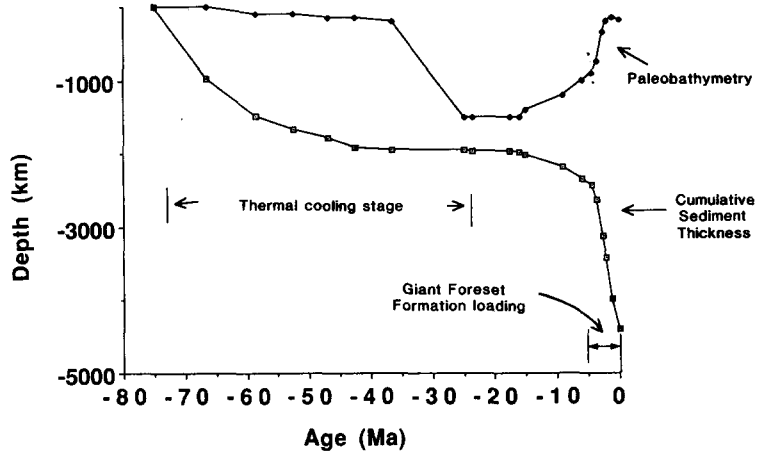

Fig. 3. Paleobathymetry and sedimentation thickness versus time for well Tane-1 located over some of the maximum thicknesses of the Giant Foreset Formation (see Fig. 4 for location). Near-constant paleobathymetry, along with exponentially decreasing sediment accumulation with time, between 75 and 40 Ma, represents thermal cooling period after the Tasman Sea rifting. Rapid subsidence, which was completed by 25 Ma, is due to subduction-related compression or foreland thrust loading [26]. Note, however, that this region received very little sediment (500 m) during the Miocene. In contrast, wells close to the Taranaki Fault received up to 4 km of sediment during the Miocene. The final 2 km of sediment deposited at Tane-1 in the last 5 Ma represents the Giant Foreset Formation loading.

Giant Foreset Formation sediment loading were set up: a depositional slope extending to a depth of over one kilometre existed at the edge of the Miocene sediment package (e.g., Fig. 4).

Plate boundary conditions changed rapidly during the Plio-Pleistocene. Compression increased southward near the termination of the Hikurangi subduction zone, the Southern Alps were uplifted [32] and the Central Volcanic Region of North Island opened up by back-arc spreading. However, since the late Eocene the Western Platform has remained free of active faulting associated with the plate boundary zone through New Zealand [16,21,32]. With the development of new topography on North and South Island, eroded sediments were deposited over the last 5 Ma onto the stable Western Platform to create the Plio-Pleistocene Giant Foreset Formation sediment package (Fig. 2).

3. Paleobathymetry and sediment isopachs

Hayward and Wood [25] determined Cenozoic paleo-seafloor depths in the region (Fig. 4) and Thrasher and Cahill [31] compiled a series of sediment isopach maps (e.g., Fig. 2) for the re-

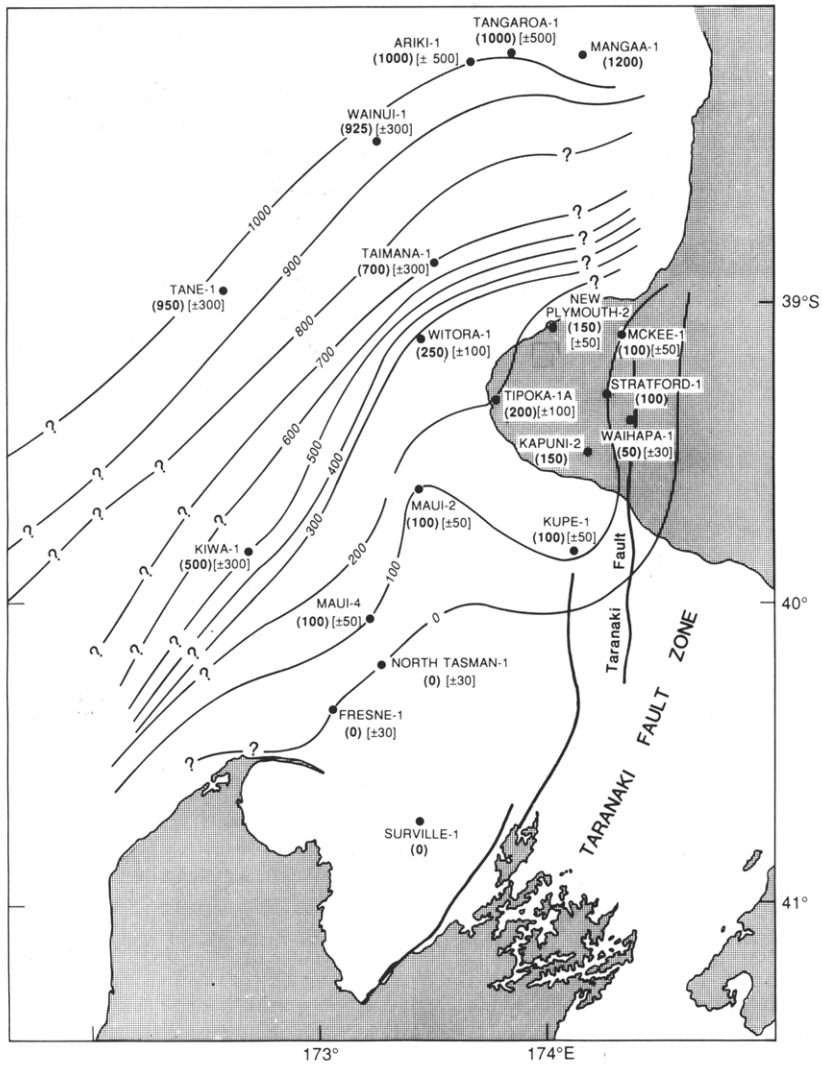

Fig. 4. Paleobathymetry map for the end of the Miocene derived from depth values [25] at well sites shown. Paleobathymetry defines the shelf onto which the Giant Foresets were deposited in the Plio-Pleistocene.

gion from the extensive seismic coverage. Paleobathymetry depths show that the Western Platform was 0.8–1.4 km below sea level just prior to the Giant Foreset sediment loading.

4. Gravity observations

Figure 5a shows the free-air gravity [33] observations over the Western Platform and Taranaki areas. A peak-to-trough gravity anomally of 35–50 mGal corresponds to the location of the Plio-Pleistocene sediment package (compare with Fig. 2). Lower gravity values southeast of the Giant Foreset Formation correspond to the Oligocene–Miocene sediment thicknesses of the Taranaki Basin and the Plio-Pleistocene Wanganui Basin. Figures 5b and 5c show two profiles across the Plio-Pleistocene sediment package (from boxes 1 and 2 in Fig. 5a) with the location of the base of Plio-Pleistocene sediments [31], the present-day bathymetry, and paleobathymetry [25]. The spatial correlation of this positive gravity anomaly with the sediment package indicates that it can be modelled to determine the isostatic response or strength properties of the lithosphere in this region.

5. Determining the load, its flexural response, and gravity signature

That part of the sediment package that fills the region between the present-day bathymetry and the paleobathymetry constitutes the load (Fig. 5b and 5c) and has a positive gravity effect. This load produces a downwarp that is filled with the remaining part of the sediment package. This infilled downwarp, along with the displaced mantle material, produces a negative gravity effect.

We use a forward modelling approach to determine the isostatic response of the sediment load. Given the paleobathymetry and the error bounds, a pre-loaded margin geometry is constructed and with this load distribution the flexural response and gravity anomaly over the structure is determined. Appropriate flexural parameters are then determined, after several modelling iterations, by the optimal match to both the structure and gravity field.

If the sediment load were completely uncompensated (e.g., infinite plate rigidity) then, using the average paleobathymetry depths of 0.8–1.4 km, the gravity over the sediment package would have a maximum of 50–80 mGal and, because no downwarp of the top of the Miocene surface could have occurred (with the exception of a small amount of compaction), the sediment package itself would only be 0.8–1.4 km thick.

The paleobathymetry of the top of the Miocene surface before sediment loading is known to within ± 50 m for shallow paleodepths and to within ± 300 m for paleodepths > 0.7 km [25] (Fig. 5b and 5c). Given the error estimates in paleodepth [25], the effective mass that loaded the margin (expressed as a 2D equivalent line-load) ranges from 1 to 2×10^{11} kg/m.

5.1. Flexural response to the load

Flexure of a thin, infinite elastic plate overlying a weak fluid can be determined by the solution to the equation:

$$D\, \mathrm{d}^4 y(x)/\mathrm{d}x^4 + \Delta\rho g y(x) = P(x) \qquad (1)$$

where $y(x)$ is the vertical displacement, g is the gravitational acceleration, $P(x)$ is the driving load (sediment load), $\Delta\rho$ is the density contrast between the material infilling the depression (caused by the load) and the mantle, and D is the flexural rigidity of the elastic plate.

The flexural rigidity, D, is defined as:

$$D = \epsilon T_e^3 / \left[12(1-\nu^2)\right] \qquad (2)$$

where ϵ is Young's Modulus and ν is Poisson's Ratio. T_e is not equivalent to lithospheric thickness, defined by seismic or heat flow observations, but is instead an effective elastic thickness that explains the flexural response of long-term vertical loads if the lithosphere were to behave as a perfectly elastic body.

Flexure from a distributed load [34] is determined using a finite difference method [35] that calculates the deflection from an arbitrarily shaped 2D mass (shape of the present-day bathymetry minus the paleobathymetry). The resulting flexure, $y(x)$, is then added to the paleobathymetry to determine the predicted shape of the top of the Miocene surface. Flexural displacement is also added to the position of the crust–mantle boundary. The density contrast between the mantle and infill is 1000 kg/m^3, and the effective density of the sediment load, because it

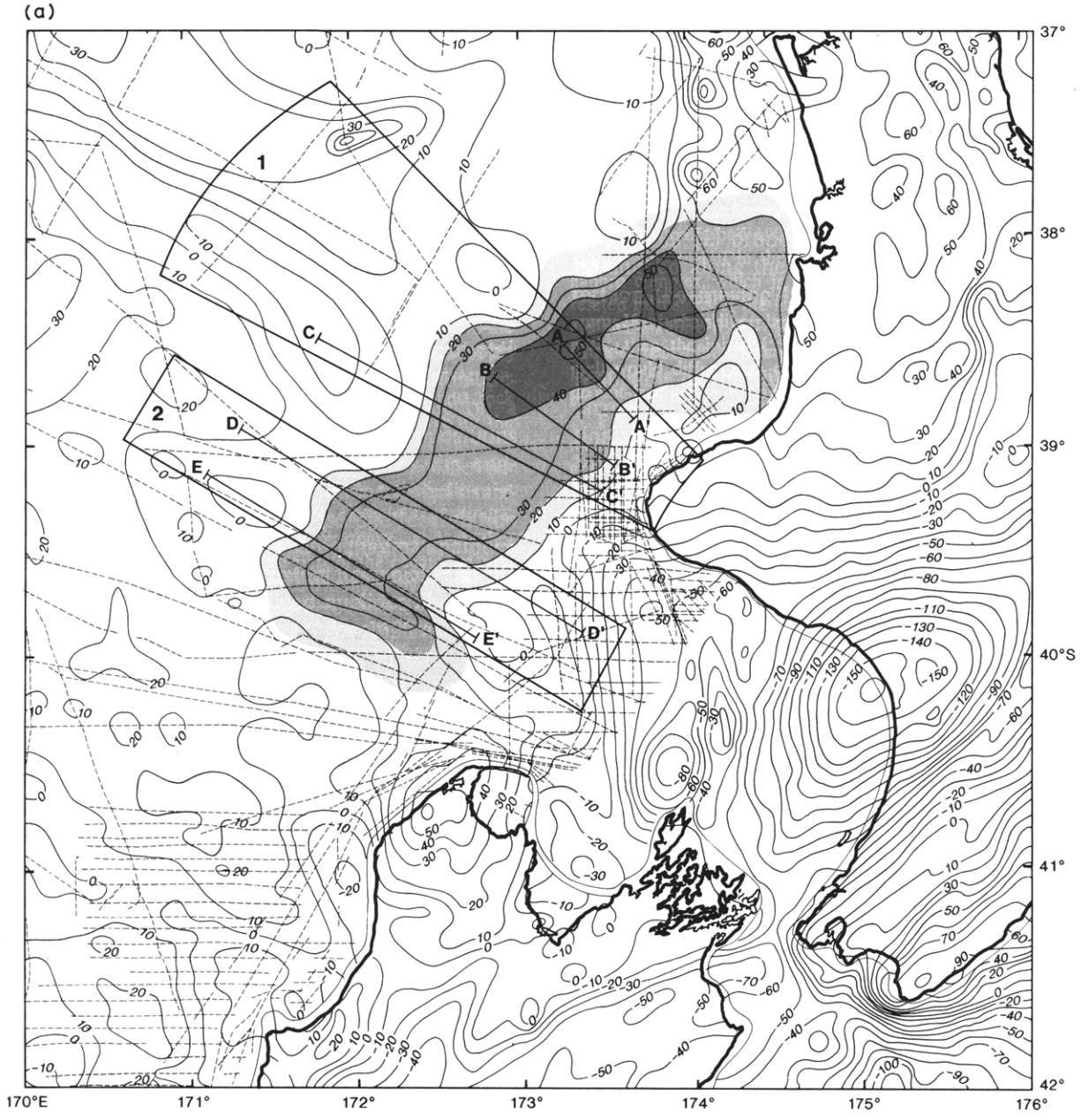

Fig. 5. (a) Free-air gravity (at sea) and Bouguer gravity (on land) [33]. Anomaly associated with Giant Foreset Formation is shaded. Note similarity in shape with isopach map (Fig. 2). Also shown are cross sections (see also Fig. 2) along which structure (top of Miocene) was averaged and boxes 1 and 2 from which gravity values in Fig. 5b, 5c, 8a and 8b were taken. Ship tracks where gravity surveys have been conducted (thin dashed lines) are shown in the region of Giant Foreset Formation. (b) Gravity values from box 1 in Fig. 5a, showing present-day bathymetry, paleobathymetry, and structure of top-Miocene surface [31] (from profiles A–A', B–B' and C–C'). Paleobathymetry depths greater than 700 m have uncertainties of ±300 m. The part of the sediment package between paleobathymetry and present-day bathymetry is defined as the load, and the remaining part of the package is infill. In a forward modeling sense, this load was adjusted to fit both the gravity and the flexure. (c) Gravity values from box 2 in Fig. 5a, with present-day bathymetry, paleobathymetry, and top-Miocene (averaged cross sections D–D' and E–E').

is immersed in water, is 1400 kg/m^3. A density of 2800 kg/m^3 is used for the crust, and 3400 kg/m^3 for the mantle.

5.2. Calculating the gravity response

The two-dimensional gravity response is computed using the line integral method [36]. By summing two effects the anomaly over the loaded shelf margin can be computed: (1) the initial edge effect produced by a compensated pre-loaded margin (Fig. 6a) and (2) the load effect (positive) and the corresponding compensating effects (negative). The sum of these two anomalies (Fig. 6b) produces a high over the sediment and a corresponding low seaward of the shelf break [see 37,38,5,15]. In this example, the pre-loaded shelf geometry is assumed to be in local compensation. The integrated gravity effect over a compensated

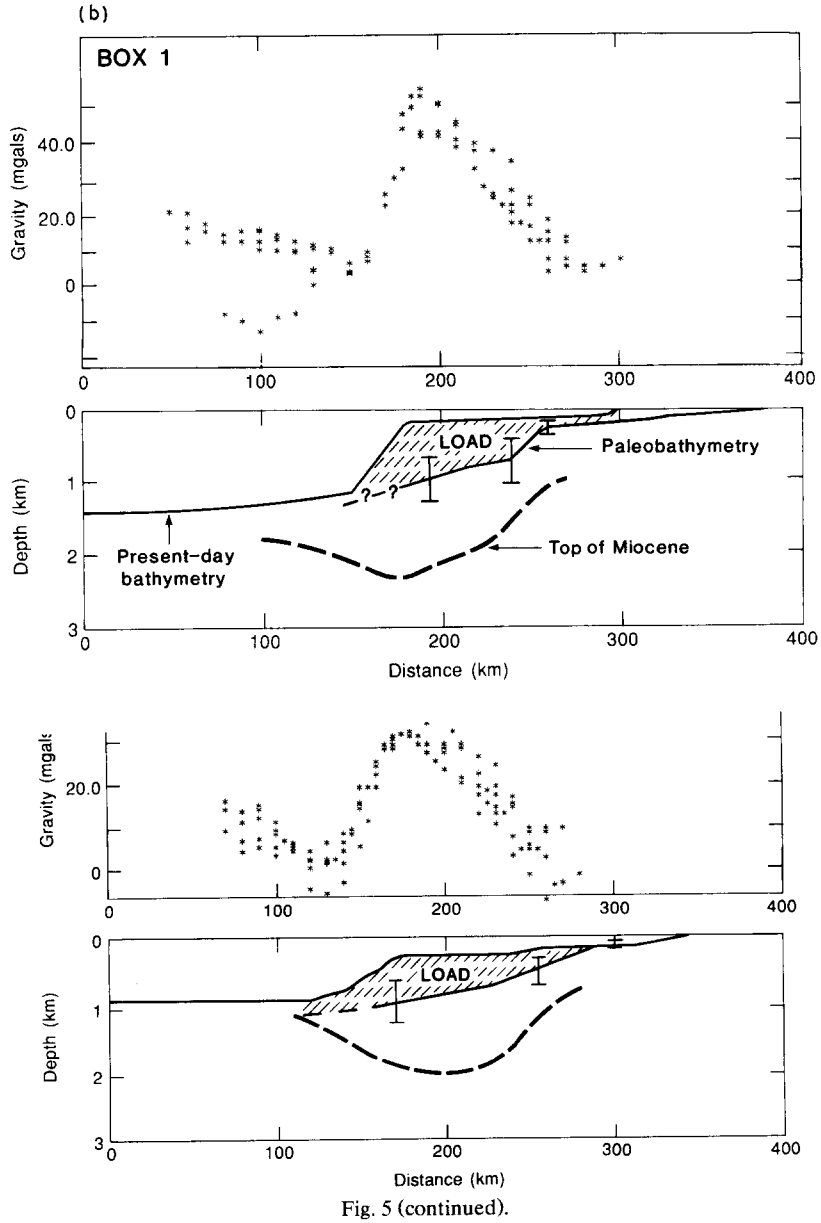

Fig. 5 (continued).

load, whether that compensation is local or regional, will always be zero.

5.3. Assumptions about compensation of pre-loaded margin and their effects on the gravity signature

Although the region of the Western Platform was substantially stretched in the Late Cretaceous, the actual margin geometry or slope upon which the Giant Foreset Formation was deposited was created by Miocene sedimentation, rather than by extension during the Late Cretaceous. Initial conditions, therefore, need not involve a margin that was compensated locally. The gravity signatures for a loaded regionally compensated margin and a loaded locally compensated margin are shown in Fig. 7. The regionally compensated margin was computed using an effective elastic thickness of 25 km. Flexural response to the sediment load for both margins was computed using $T_e = 25$ km. Figure 7 shows that the absolute amplitude and shape of the gravity anomaly for both loaded margins is very close over the sedimetary load. We will show in the next section that it is the relative peak-to-trough amplitude and the shape of the anomally over the centre of the load that is important for constraining the isostatic response. Therefore, the initial compensation mechanism of the pre-loaded margin has only a minor influence on the important part of the gravity signature for a load of this size. For simplification we therefore assume for all calculations that the margin was locally compensated before sediment loading.

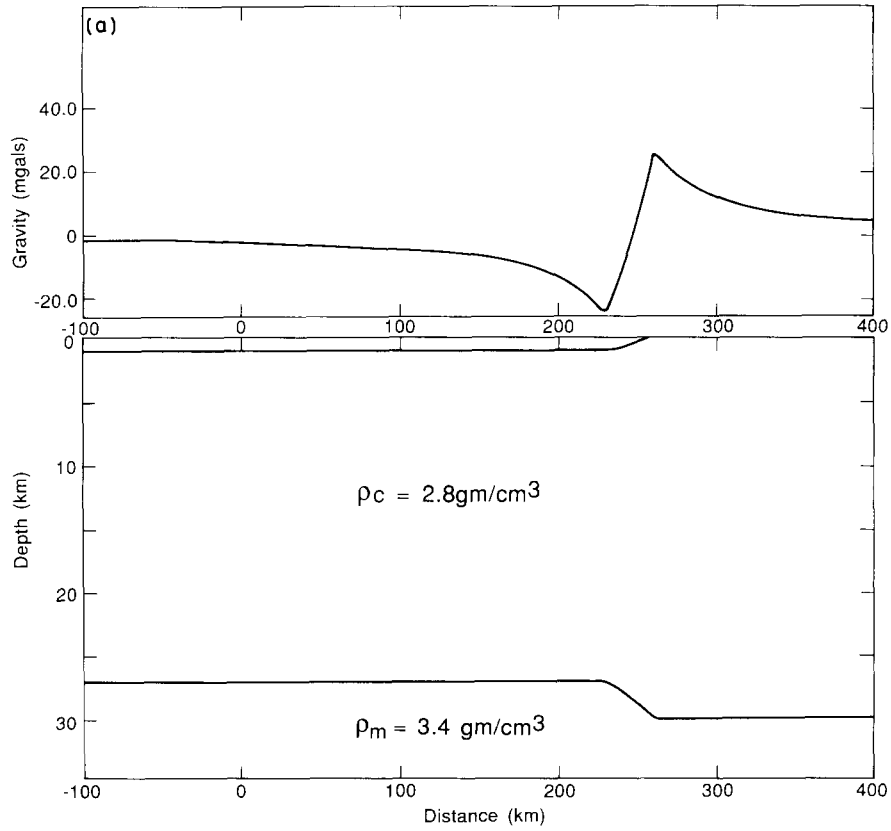

Fig. 6. Computation of gravity anomaly over sediment-loaded shelf margin. (a) Initial edge-effect anomaly over paleoshelf margin; water depth = 1.4 km. Shelf margin is assumed here to be initially in local isostatic compensation. (b) Complete effect including the initial edge effect, the positive load of sediments that replaced water, and the negative effect of the infilled depression and displaced mantle. Gravity anomaly over the load integrates to zero. Sediment load shown has an equivalent line load mass of 1.4×10^{11} kg/m. Flexure for this example was calculated using the distributed load shown and a T_e of 20 km.

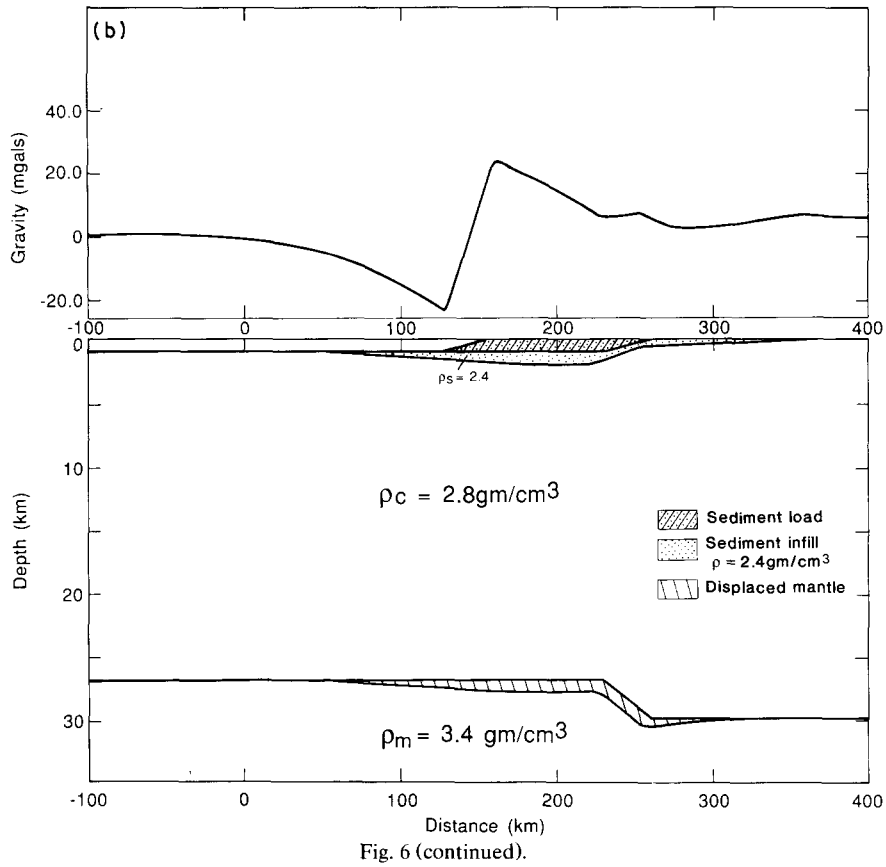

Fig. 6 (continued).

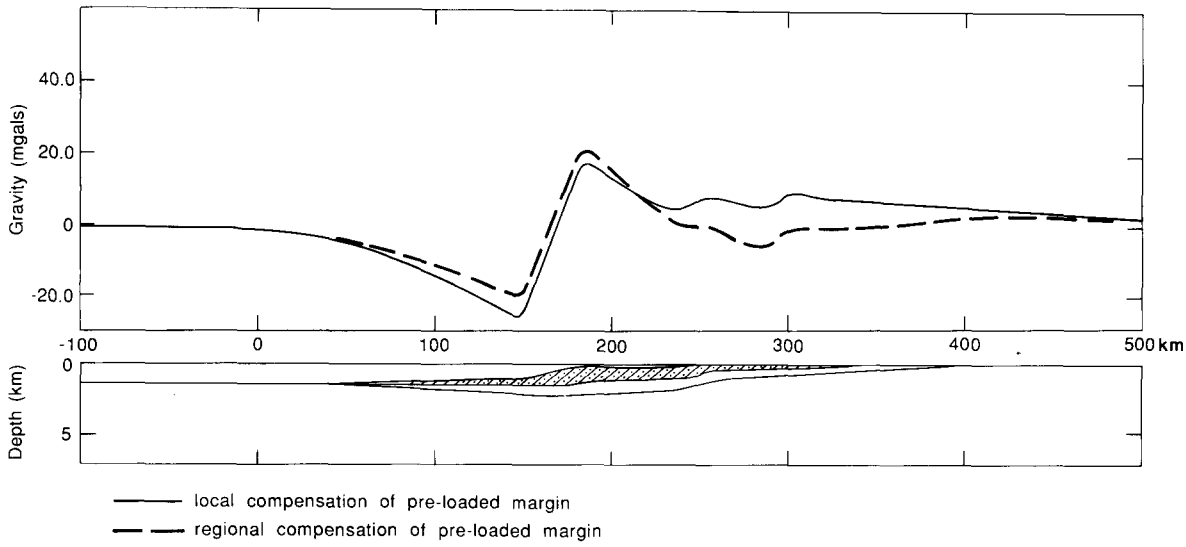

Fig. 7. Two gravity anomalies over a sedimentary load that was deposited on a locally compensated margin (solid line) and a regionally compensated margin (dashed line). Flexural response to the sedimentary load in this example is for $T_e = 25$ km for both cases. The flexural response on the Moho is not shown. The important parts of the anomaly—high over the shelf break and low over shelf base—are roughly equal for both margins (identical relative peak-to-trough values). This figure demonstrates that the initial compensation mechanism of the pre-loaded shelf margin (for a load of this size) is relatively unimportant in constraining the isostatic response to a sedimentary load.

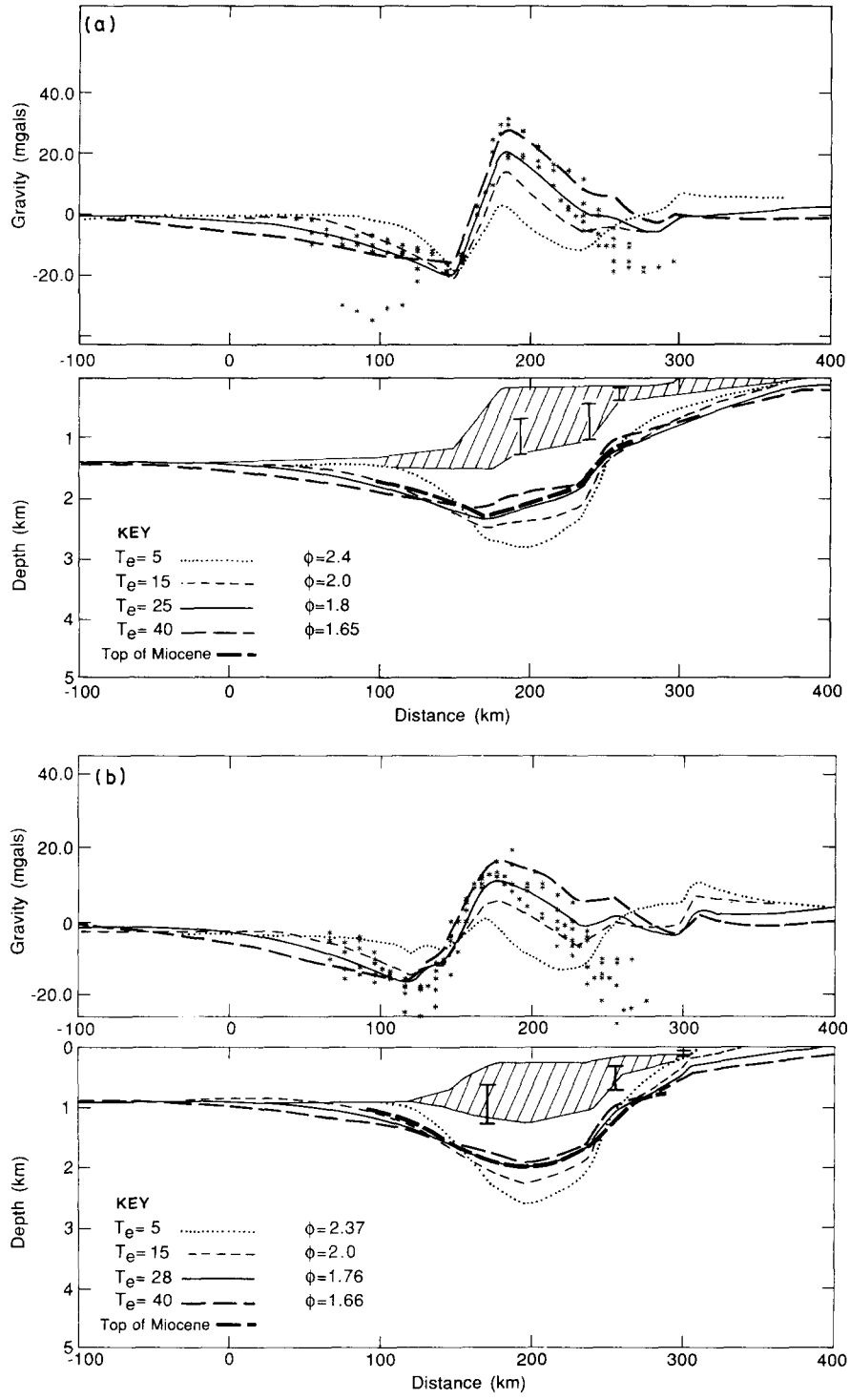

Fig. 8. Gravity and flexure model results over the regions in boxes 1 and 2 (Fig. 5a). Sediment load (shaded) for both profiles is the mass distribution that gave best match to both structure (top of Miocene) and gravity. Original error bars of paleoshelf bathymetry (from Fig. 5b and 5c) are shown. A low rigidity ($T_e = 5$ km) provides a poor match to both structure and gravity. An elastic thickness of about 25 km provides the best match to both the observed gravity anomaly and the flexed Miocene/Pliocene boundary. The sediment package over region of box 1 has an effective mass (expressed as equivalent line load) of 2×10^{11} kg/m. The mass over the region of box 2 is 1.45×10^{11} kg/m. Not shown, but incorporated into gravity calculations, is the flexural response on the Moho. The amplification factors ϕ (see Fig. 10) for each elastic thickness used are shown. These factors are in close agreement with those predicted by the analytical solution for a load of 100 km in width (eqn. 3, Fig. 10b). The optimal solution is given by $T_e = 25$ km for box 1 (Fig. 8a) and $T_e = 28$ km for box 2 (Fig. 8b).

5.4. Results

Figures 8a and 8b show the gravity response and flexure for the load, within regions 1 and 2 of Fig. 5a respectively, for several values of T_e. Low values of T_e (5 km) provide a poor match to both structure and gravity in comparison to higher values ($T_e = 25$ km). In order to match the peak-to-trough amplitude of the gravity anomaly over the sediment package in both regions 1 and 2, maximum loads, close to the bottom of the error estimates in paleobathymetry, and T_e values greater than 20 km are required. No combination of load and flexural response could match both gravity and structure when low rigidities ($T_e = 5$–10 km) were used.

Because the region of the Giant Foreset Formation is underlain by up to 3 km of Cretaceous–Miocene sediments, differential sediment compaction is another factor to consider: not all of the displacement of the top of the Miocene interface may be due to flexure. From wet density and particle density values of Cretaceous to Miocene sedimentary rocks [39] the maximum amount of compaction expected is about 6–9% of the column (ca. 200 m). Scatter in the gravity data does not allow us to resolve small differences in plate deflection of this order, but it is important to note that if effects of compaction were known and included, larger estimates of flexural rigidity would be forced.

Gravity observations on the eastern side (right-hand side of Fig. 8a and b) of the sediment package are lower than those predicted by the model. These lower gravity values are due to a thickening wedge of predominently Miocene sediments in the Taranaki Foreland Basin [26] and are unrelated to the isostatic response of the Plio-Pleistocene sediment load. Most important, in terms of constraining the flexural response to the load, is to match the anomaly over the centre of the load, and to match the maximum, which lies over the present-day shelf break, and the minimum, which lies at the base of the shelf margin. The Miocene wedge will, therefore, have a minimal influence on the part of the gravity that is critical in resolving the rigidity beneath the Giant Foresets. Figure 9 demonstrates this point, and shows that by including the effect of the foreland basin wedge of Oligocene–Miocene sediments [31] the complete gravity anomaly (using

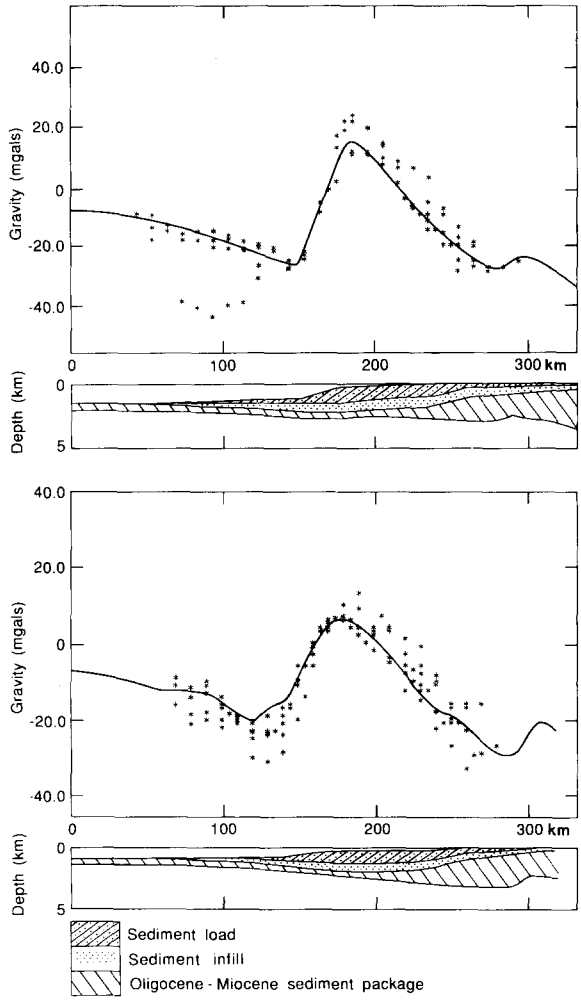

Fig. 9. Best-fit models from Fig. 8a and 8b ($T_e = 25$ km) for regions in boxes 1 and 2 (Fig. 5a) with an allowance for the gravity effect of the Oligocene–Miocene sediment wedge associated with the Taranaki Foreland Basin.

the best fit T_e from Fig. 8a and 8b) out to the east can be matched. In summary, the match to the gravity anomaly over the Giant Foreset Formation shelf break and base of shelf margin, as well as the match of the flexural response to the structure, demonstrates that the lithosphere in this part of the New Zealand continent displays a finite strength.

6. Resolution: flexure

The large, thick (ca. 12–15 km) sedimentary loads that have accumulated on old (200–150 Ma) Atlantic-type margins have been the subject

of important studies demonstrating the character of isostatic compensation [e.g., 37,38,5,15]. These loads are impressive, as they typically produce peak-to-trough free-air gravity anomalies of 100 mGal, which are substantially greater than the background variations of 10–20 mGal typically found over oceans and continents. The signal-to-noise ratio, although important, is not the only consideration in modelling rigidity from sedimentary loads at a continental margin. Resolution is also important.

Resolution is here qualitatively defined as the change in isostatic response, or observed gravity anomaly, over the centre of the load as a function of changes in the elastic parameters. The isostatic response of a load and its dependence on load wavelength is well known and has been demonstrated in isostatic admittance studies [40–42], coherence studies [43,9], and in the spatial domain for a visco-elastic model [44] and an elastic model [45,46], where in the elastic case the loading function is periodic. Of relevance in this study is to consider the isostatic response for a load of finite width. In particular we consider the amplification factor $\phi = (Y + H)/H$ [45] (see Fig. 10a), which is the ratio of maximum amplitude after loading ($Y + H$ = isopach thickness) to the amplitude before loading (paleobathymetry = H), and determine how ϕ changes as a function of load width. Using the solution for flexural displace-

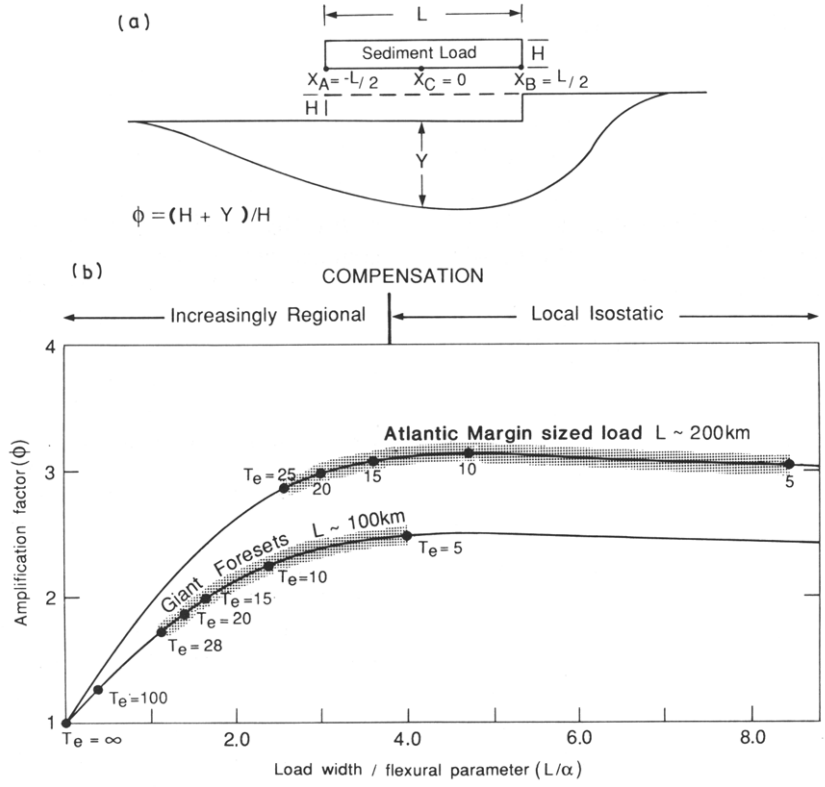

Fig. 10. (a) Amplification factor ϕ for a sediment-loaded shelf margin is the ratio of the isopach thickness ($Y + H$) to the original water depth (H) that was replaced by sediments. The parameter Y is the magnitude of the flexural response beneath the centre of the load. (b) Graph of amplification factor ϕ versus the dimensionless ratio L/α (load width over flexural parameter). Bottom curve is for Giant Foreset load (sediment density = 2400 kg/m^3); top curve is for an older, larger load (sediment density = 2600 kg/m^3), like the North American Atlantic margin. Curves show that if the load width L is at least four times greater than the flexural parameter α, the maximum displacement is attained beneath the centre of load. The range of amplification values (for given range of elastic thicknesses of 5–25 km) for both loads is highlighted. Best resolution for T_e occurs for L/α ratios between 1.0 and 3.0, where ϕ as a function of T_e changes rapidly. When T_e is in the range 5–25 km, this rapid change is more apparent for loads 100 km wide than for loads 200 km wide.

ment directly beneath the centre of a distributed load of width L [34], the amplification factor can be expressed as:

$$\phi = \rho_L/(\rho_m - \rho_f)\left[1 - e^{-L/2\alpha}\cos(L/2\alpha)\right] + 1 \quad (3)$$

where ρ_L is sediment density, ρ_m is mantle density, ρ_f is infill density, g is gravitational acceleration and $\alpha = [4D/((\rho_m - \rho_f)g)]^{1/4}$ is the flexural parameter [3], and has units of length. Using a load density of 1400 kg/m^3, an infill density of 2400 kg/m^3 and a mantle density of 3400 kg/m^3, the amplification factor for the Giant Foresets, for perfect local isostasy, is 2.4.

Figure 10b shows a graph of the amplification factor as a function of the dimensionless ratio of load width, L, to the flexural parameter, α. Any load width four times greater than the flexural parameter provides a compensation that can be considered near local isostasy (maximum amplification beneath the centre of the load). The second curve in Fig. 10b shows the range of amplification for an Atlantic margin-type sedimentary load [37,38,5,15], which would have a width of 200 km or greater, and a higher average infill density of 2600 kg/m^3. Flexural properties can be best resolved if, for a given load width, the range of rigidities, or elastic thicknesses, falls on the steep, upper part of the amplification factor curve (location of Giant Foresets). The load width of the Giant Foreset sediments is therefore optimal for resolving flexural rigidity if the lithosphere in the region is characterised by T_e values in the range 5–25 km. Analyses of Atlantic-type passive margins are evidently best suited for resolving T_e values greater than about 20 km, but are poorly suited for resolving differences in values less than $T_e = 15$ km.

6.1. *Resolution: gravity*

Because gravity anomalies over loads are dependent on the amount of isostatic amplification, the normalised gravity over the centre of the load will also be a function of the ratio L/α (Fig. 11). The curve in Fig. 11 is not the same for all values of L because of the gravity edge effects, but gravity is plotted here as a function of L/α to aid comparison with Fig. 10b. The two curves shown are for loads of 100 and 200 km in width, and relevant elastic thickness values (5–25 km) are indicated. Note that for the slab of 100 km in width the gravity over the centre of the load changes rapidly for the effective elastic thickness range of 5–25 km. For the 200 km wide load, however, appreciable changes in gravity over the

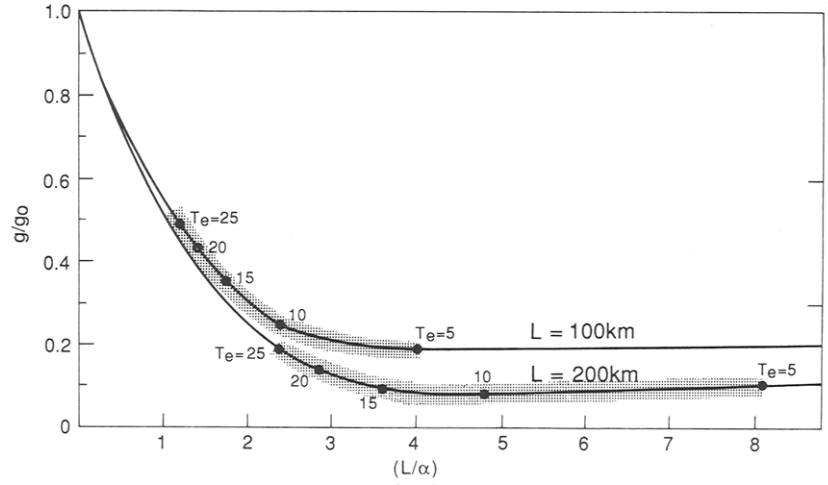

Fig. 11. Gravity over centre of slab of thickness H and width L (normalised by its Bouguer slab gravity) as a function of dimensionless ratio L/α. Curves for $L = 100$ km and $L = 200$ km are shown and T_e values are indicated. For a 100 km wide load, gravity over the centre of the load varies significantly for T_e between 5 km and 25 km. Less variation in gravity occurs for 200 km wide loads for T_e in this range, particularly for values of T_e less than 15 km.

centre of the load only occur for elastic thickness values greater than 15 km.

The important point to be gained from this discussion on resolution is that large loads do not, by virtue of their high signal-to-noise ratio, necessarily represent more favourable conditions for resolving T_e than smaller loads. For elastic thicknesses in the range of 5–25 km, the resolution is optimal for a narrow load (80–110 km) such as the Giant Foresets.

7. Discussion

Our results from the Western Platform are consistent with those of Karner and Watts [5], who obtained a $T_e < 5$ km for the submarine continuation of the New Zealand continent, the Lord Howe Rise Margin (Fig. 1). In the region where their profiles are located, 1200 km northwest of North Island, the margin contains very little post-rift sediment and the state of isostasy therefore reflects the strength of the region at the time of rifting [5]. In contrast, the Plio-Pleistocene sedimentation of the Giant Foresets was not related to rifting. Instead, sedimentation began with the development of the Pacific/Australian plate boundary, with subsequent uplift and mountain building 70 Ma after rifting. Hence, the T_e determined from the Giant Foreset loading relates to lithosphere with a thermal age of at least 70 Ma. Therefore, the comparison of the results from the Lord Howe Rise [5] and the Giant Foresets provides a useful view of how rigidity at a single margin, which has remained free of significant post-rift faulting, has increased from a low value of $T_e < 5$ km at the time of rifting, to an intermediate value ($T_e = 20$–30 km) 70–80 Ma after rifting. This result is in keeping with rigidity being controlled by the 450 °C isotherm of a cooling half-space model [13].

There is an apparent contradiction between our results for a lithosphere with appreciable strength (in response to vertical loads) and those observations to the east, within the plate boundary zone of central New Zealand, that show, for wavelengths of observation at horizontal distances greater than 40 km, a continental lithosphere deforming in the horizontal dimension more or less as a continuum [47,48]. These apparently disparate observations can be explained in two ways: (1) the region of Giant Foreset Formation loading is sufficiently far from the plate boundary zone that it has remained unaffected by the distributed strain, thus allowing the region to acquire a finite strength, or (2) the continental lithosphere responds differently to horizontal loads compared to vertical loads because of its rheological layering [49–52]. A well-constrained estimate of the rigidity within the deforming part of the New Zealand continental lithosphere is needed to test these hypotheses.

8. Conclusions

The two principal conclusions of this study are as follows:

(1) Effective elastic thicknesses for the continental lithosphere of the western margin of New Zealand, which has a thermal age of 70–80 Ma, are in the range $T_e = 20$–30 km.

(2) Narrow (ca. 100 km), rapidly deposited sedimentary loads at continental margins, which are of a sufficient thickness to produce a viable gravity anomaly, offer a high resolution for the determination of T_e when T_e is in the range 5–25 km.

Acknowledgements

We are grateful to Dick Walcott (Victoria University of Wellington) and Clem Chase (University of Arizona) for discussion, review, and comments on earlier versions of this paper. Ray Wood (DSIR, Geology and Geophysics) also provided a helpful review of the revised manuscript. We also appreciate discussions, ideas and a review shared by Glen Thrasher (DSIR, Geology and Geophysics). Carolyn Hume provided helpful assistance with the drafting of the figures.

References

1 A.B. Watts, J.H. Bodine and M.S. Steckler, Observations of flexure and state of stress in oceanic lithosphere, J. Geophys. Res. 85, 6369–6376, 1980.
2 M.K. McNutt, M. Diament and M.G. Kogan, Variations of elastic plate thickness at continental thrust belts, J. Geophys. Res. 93, 8825–8838, 1988.
3 R.I. Walcott, Flexural rigidity, thickness and viscosity of the lithosphere, J. Geophys. Res. 75, 3941–3954, 1970a

4 R.I. Walcott, Isostatic response to loading of the crust in Canada, Can. J. Earth Sci. 7, 716–727, 1970b.
5 G.D. Karner and A.B. Watts, On isostasy at Atlantic-type continental margins, J. Geophys. Res. 87, 2923–2948, 1982.
6 G.D. Karner and A.B. Watts, Gravity anomalies and flexure of the lithosphere at mountain ranges, J. Geophys. Res. 88, 10449–10477, 1983.
7 H. Lyon-Caen and P. Molnar, Constraints on the structure of the Himalaya from an analysis of gravity anomalies and a flexural model of the lithosphere, J. Geophys. Res. 88, 8171–8192, 1983.
8 M.T. Zuber, T.D. Bechtel and D.W. Forsyth, Effective elastic thicknesses of the lithosphere and mechanisms of isostatic compensation in Australia, J. Geophys. Res. 94, 9353–9367, 1989.
9 T.D. Bechtel, D.W. Forsyth and C.J. Swain, Mechanisms of isostatic compensation in the vicinity of the East African Rift, Kenya, Geophys. J.R. Astron. Soc. 90, 445–465, 1987.
10 J.A. Nunn and N.H. Sleep, Thermal contraction and flexure of basins: a three dimensional study of the Michigan basin, Geophys. J.R. Astron. Soc. 76, 587–635, 1984.
11 T.A. Stern and U.S. ten Brink, Flexural uplift of the Transantarctic Mountains, J. Geophys. Res. 94, 10315–10330, 1989.
12 P. Molnar and P. Tapponnier, A possible dependence of tectonic strength on the age of the crust in Asia, Earth Planet. Sci. Lett. 52, 107–114, 1981.
13 G.D. Karner, M.S. Steckler and J.A. Thorne, Long-term thermo-mechanical properties of the continental lithosphere, Nature 304, 250–253, 1983.
14 S. Fowler and D. McKenzie, Gravity studies of the Rockall and Exmouth Plateaux using SEASAT altimetry, Basin Res. 2, 27–34, 1989.
15 Watts, A.B. Gravity anomalies, crustal structure and flexure of the lithosphere at the Baltimore Canyon Trough, Earth Planet. Sci. Lett. 89, 221–238, 1988.
16 W.F.H. Pilaar and L.L. Wakefield, Structural and stratigraphic evolution of the Taranaki Basin, offshore North Island, New Zealand, Aust. Assoc. Pet. Geol. J. 18, 93–101, 1978.
17 K.B. Sporli, Development of the New Zealand Microcontinent, in: Circum-Pacific Ocean Basin, J.W.H. Monger and J. Francheteau, eds., AGU Geodyn. Ser. 18, 115–132, 1977.
18 A. Wodziki, Geology of the pre-Cenozoic basement of the Taranaki–Cook Strait–Westland area, New Zealand, based on recent drillhole data, N.Z.J. Geol. Geophys. 17, 747–757, 1974.
19 J.K. Weissel, D.E. Hayes and E.M. Herron, Plate tectonic synthesis: the displacements between Australia, New Zealand and Antarctica since Late Cretaceous, Mar. Geol. 25, 231–277, 1977.
20 R.M. Carter and R.J. Norris, Cainozoic history of southern New Zealand: An accord between geological observations and plate-tectonic predictions, Earth Planet. Sci. Lett. 31, 85–94, 1976.
21 G.J. Knox, Taranaki Basin, structural style and tectonic setting, N.Z.J. Geol. Geophys. 25, 125–140, 1982.
22 P.R. King and G.P. Thrasher, Post-Eocene development of the Taranaki Basin, New Zealand: Convergent overprint of a passive margin, in: Continental Margins, D.G. Halbouty, ed., AAPG Mem., in press, 1991.
23 M.G. Laird, The late Mesozoic fragmentation of the New Zealand segment of Gondwana, in: Gondwana Five. Proceedings of the Fifth International Gondwana Symposium, Wellington, New Zealand, M.M. Cresswell and P. Vella, eds., pp. 311–318, 1980.
24 A.J. Tulloch and D.L. Kimbrough, The Paparoa metamorphic core complex, New Zealand: Cretaceous extension associated with fragmentation of the Pacific margin of Gondwana, Tectonics 8, 1217–1234, 1989.
25 B.W. Hayward and R.A. Wood, Computer-generated geohistory plots for Taranaki drillhole sequences, N.Z. Geol. Surv. Rep. PAL 147, 1989.
26 T.A. Stern and F.J. Davey, Deep seismic expression of a foreland basin: Taranaki basin, New Zealand, Geology 18, 979–982, 1990.
27 D.P. McKenzie, Some remarks on the development of sedimentary basins, Earth Planet. Sci. Lett. 40, 25–32, 1978.
28 P.R. King and P.H. Robinson, An overview of Taranaki region geology, N.Z. Energy Explor. Exploit. 6, 213–232, 1988.
29 P.F. Ballance, Evolution of the upper Cenozoic magmatic arc and plate boundary in northern New Zealand, Earth Planet. Sci. Lett. 28, 356–370, 1976.
30 G. Rait, F. Chanier and D.W. Waters, Landward- and seaward-directed thrusting accompanying the onset of subduction beneath New Zealand, Geology, 19, 230–233, 1991.
31 G.P. Thrasher and J.P. Cahill, Subsurface maps of the Taranaki Basin, New Zealand, N.Z. Geol. Surv. Rep. G-142, 1990.
32 R.I. Walcott, Geodetic strain and the deformational history of the North Island of New Zealand during the late Cainozoic, Philos. Trans. R. Soc. London, A321, 163–181, 1987.
33 K.H. Rose, Cook gravity anomaly map. Oceanic series, 1:1000000, DSIR, Wellington, 1990.
34 M. Hetenyi, Beams on an Elastic Foundation, Univ. Michigan Press, Ann Arbor, 1946.
35 J.H. Bodine, M.S. Steckler and A.B. Watts, Observations of flexure and the rheology of the oceanic lithosphere, J. Geophys. Res, 86, 3695–3707, 1981.
36 M. Talwani, Computer usage in the computation of gravity anomalies, Math. Comput. Phys. 13, 343–389, 1973.
37 R.I. Walcott, Gravity, flexure and growth of sedimentary basins at a continental edge, Geol. Soc. Am. Bull. 83, 1145–1848, 1972.
38 J.R. Cochran, Gravity and magnetic investigations in the Guiana Basin, Western Equatorial Atlantic, Geol. Soc. Am. Bull. 84, 3249–3268, 1973.
39 T. Hatherton and A.E. Leopard, The densities of New Zealand rocks, N.Z.J. Geol. Geophys. 7, 605–614, 1964.
40 B.T.R. Lewis and L.M. Dorman, Experimental Isostasy, 2, an isostatic model for the USA derived from gravity and topography data, J. Geophys Res. 75, 3367–3386, 1970.

41 D.P. McKenzie and C. Bowin, The relationship between bathymetry and gravity in the Atlantic Ocean, J. Geophys. Res. 81, 1903–1915, 1976.
42 M.K. McNutt and R.L. Parker, Isostasy in Australia and the evolution of the compensation mechanism, Science 199, 773–775, 1978.
43 D.W. Forsyth, Subsurface loading and estimates of the flexural rigidity of continental lithosphere, J. Geophys. Res. 90, 12623–12632, 1985.
44 C. Beaumont, The evolution of sedimentary basins on a viscoelastic lithosphere: theory and examples, Geophys. J.R. Astron. Soc. 55, 471–497, 1978.
45 R.I. Walcott, An isostatic origin for basement uplifts, Can. J. Earth Sci. 7, 931–937, 1970c.
46 D.L. Turcotte and G. Schubert, Geodynamics. Applications of Continuum Physics to Geological Problems, Wiley, 1982.
47 H.M. Bibby, Geodetically determined strain across the southern end of the Tonga–Kermadec–Hikurangi Subduction Zone, Geophys. J.R. Astron. Soc. 66, 513–533, 1981.
48 R.I. Walcott, The kinematics of the plate boundary zone through New Zealand: a comparison of short- and long-term deformations, Geophys. J.R. Astron. Soc. 79, 613–633, 1984.
49 R. Meissner and Th. Wever, Lithospheric rheology: continental versus oceanic units, J. Petrol., Spec. Lithosphere Iss., 53–61, 1988.
50 W. Brace and D. Kohlstedt, Limits of lithospheric stress imposed by laboratory experiments, J. Geophys. Res. 85, 6245–6252, 1980.
51 N.J. Kusznir and D.H. Mathews, Deep seismic reflections and the deformational mechanics of the continental lithosphere, J. Petrol., Spec. Lithosphere Iss., 63–87, 1988.
52 P. Molnar, Continental tectonics in the aftermath of plate tectonics, Nature 335, 131–137, 1988.
53 Plate tectonic map of the Circum-Pacific region, southwest quadrant, Am. Assoc. Pet. Geol., 1981.